

**IMPROVING ENERGY DENSITY AND RESPONSE
TIME OF SUPERCAPACITORS THROUGH
ELECTROCHEMICAL TREATMENT AND DEFECT
ENGINEERING**

RUPESH M TAMGADGE



**DEPARTMENT OF CHEMICAL ENGINEERING
INDIAN INSTITUTE OF TECHNOLOGY DELHI**

JUNE 2020

©Indian Institute of Technology Delhi (IITD), New Delhi, 2020

Improving Energy Density and Response Time of Supercapacitors Through Electrochemical Treatment and Defect Engineering

by

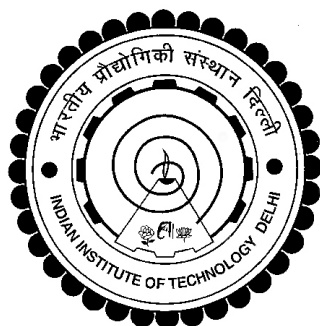
Rupesh M Tamgadge

Department of Chemical Engineering

Submitted

in fulfillment of the requirements of degree of Doctor of Philosophy

to the



Indian Institute of Technology Delhi

June 2020

*- I would like to dedicate my thesis to my beloved grandparents for
teaching me the importance of education in life -*

Certificate

This is to certify that the thesis entitled “**Improving Energy Density and Response Time of Supercapacitors Through Electrochemical Treatment and Defect Engineering** ” submitted by **Mr. Rupesh M Tamgadge** to the Indian Institute of Technology Delhi, for the award of the degree of **Doctor of Philosophy** in Chemical Engineering, is a record of bonafide research work carried out by him. Mr. Rupesh M Tamgadge has worked under my guidance and supervision and has fulfilled the requirements for the submission of the thesis. The results contained in this thesis have not been submitted in part or in full to any other university or institute for the award of any degree or diploma.



Anupam Shukla
Department of Chemical Engineering
Indian Institute of Technology, Delhi
India - 110016.

Acknowledgments

Undertaking a PhD has been a truly transformative experience for me and it would not have been possible without the blessings of Baba and support and guidance of many people.

Firstly, I am grateful to my thesis supervisor, Prof. Anupam Shukla for his guidance, motivation, and patience throughout the research work. Since the first day of my Ph.D, he helped me a lot, right from selecting courses of study to post Ph.D carrier tips. I remember the day, in Summer 2015, while performing my first experiment with two graphite sheets, he taught me how to use multimeter. It was the actual starting point of my research in this new area of electrochemical energy storage. Under his supervision, I have learnt how to define a research problem, find a solution to it, and finally publish results. On personal level, I have learnt extensively from him, be his time management, way of handling students, work ethics, etc. To summarize, most of the credit of this research work output goes to him.

I would like to express my gratitude to Prof. Anil Verma, Prof. M. Ali Haider and Prof. Pravin Ingole (Chemistry department) and all other faculty members of Chemical Engineering Department, IIT Delhi for their technical guidance and encouragement.

I wish to acknowledge my lab-mates, Ms. Isha Atrey, Mr. Rahul Raghuwanshi, Mr. Satirth Sarma, Mrs. Pooja Jangir, UG and PG juniors Aman, Apoorva, Pooja, Abhilesh, Deepak, Sumit for their help and moral support throughout this journey. I also wish to acknowledge my seniors Dr. Afkham Mir, Dr. Jay Pandey, Dr. Hundessa, and supporting staff of Chemical Engineering Department, for their valuable inputs. I also like to acknowledge central research facilities (CRF and NRF) of IIT Delhi, XPS facility of IIT Kanpur, EPR characterization lab JNU Delhi, Prof. K K Pant's, and Prof Anil Verma's lab for providing material characterization facilities.

Finally, I would like to express my sincere gratitude to peoples who mean the most to me, my grandparents, parents, brother, sister, Jiju, Arnav for their selfless love, support, and motivation. Last but not the least, my friends, specially, Nikhil, KT and Ruchi for their constant support and encouragement through ups and downs of this long journey of getting a Ph.D.



Rupesh M Tamgadge

Abstract

Supercapacitor is a class of electrochemical energy storage device that show a variation in the potential with the amount of charge stored. It is ideally suited to applications requiring pulse power, such as emergency opening of doors in jet planes, regenerative braking in automobiles, etc. It bridges the gap between the conventional dielectric capacitor and a battery. It has higher energy density as compared to a dielectric capacitor and larger power density, cyclic life compared to a battery. However, commercial applications of supercapacitors is limited by very small energy density that is an order of magnitude smaller than a battery. Further, the requirement of higher energy and power density on the storage device is rising with the continuous improvement and increase in features modern portable and flexible electronic gadgets and other applications. Research to improve the energy density of supercapacitor is primarily focused on developing better electrode materials. The strategies depend on the type of supercapacitor. For an electric double layer capacitor, the effort is on developing electrodes with high specific surface area without compromising on the electronic conductivity. For a pseudocapacitor electrode, apart from the surface area improvement in electronic conductivity of the semi-conducting active material is also a prime focus. Another direction in the supercapacitor research is to improve the frequency response of the device. Most-

supercapacitor show capacitive behavior up to 5 Hz signal frequency and there's is a huge scope for fast frequency response supercapacitor for filtering applications at high frequency which are currently employ bulky electrolytic capacitor.

In this work, I aimed to improve the energy density (based on total weight of a device) and frequency response of supercapacitors through electrochemical treatment and defect engineering. In the first experimental study, a commercially available highly oriented pyrolytic graphite sheet was partially exfoliated in different sulfate ion based electrolytes to get vertically oriented graphene nanoflakes morphology on the surface. Different process parameters such as current density of exfoliation, time of exfoliation, pH and concentration of the electrolyte were optimized and the best electrode showed areal capacitance of 752 mF cm^{-2} at current density of 2 mA cm^{-2} . The rate of partial exfoliation was found to be slow in low pH electrolyte solution and the obtained electrode has higher areal capacitance. It was observed that expansion of electrode play an equally important role as the open channel morphology of vertically oriented graphene nanoflakes in improving the capacitive performance.

A 2D graphite sheet can expand only along the thickness of electrode, whereas fiber paper has advantage of possible expansion of the fibers in three dimensions. Therefore, in our second study, I have used carbon fiber paper as an electrode material. The Electrochemical anodization of the carbon fiber paper was carried out in sulfuric acid solutions of different concentrations, ranging from 1 M–14 M. The characterization done show that it causes structural adjustments that expose a greater number of electrochemically active graphene edges to the surface, increases surface roughness, increases defects in graphitic structure and introduces oxygen functionality on the surface. These changes result in two orders of magnitude

increase of the surface area, and several order of magnitude increased in areal capacitance compared to pristine electrode. The areal capacitance of the anodized carbon fiber paper at the optimal conditions, 2.47 F cm^{-2} at 2 mA cm^{-2} , is 50% more than the best literature value for a carbon-based or a pseudocapacitive material-loaded carbon electrode.

The third study was on improving the capacitive performance of anatase, a pseudocapacitive material of low cost, electrochemical stability, and high theoretical capacitance, but poor electrical conductivity. A simultaneous improvement in electrical conductivity and nanostructuring was undertaken. A two step hydrothermal route was employed to dope anatase with fluorine element. Fluorine doping leads to the creation of oxygen vacancies as well as the Ti^{3+} states. Electrochemical characterizations show that these defects increase electronic charge carrier density and local conductivity of the doped anatase by an order of magnitude compared to the pristine anatase. In addition, the hydrothermal treatment lead to nanostructuring of anatase that increased the surface area by order of magnitude. As a result of the two improvements, doped anatase showed three times (236 F g^{-1}) higher specific capacitance than the pristine one and its rate capability is also better.

In the last study, the focus was to improve the frequency response of a pseudocapacitor for kilohertz frequency applications. I have fabricated a pseudocapacitor electrode with a thin anatase layer of open pore morphology by anodization of a titanium sheet in NH_4F solution. Electrochemical reduction was performed to improve the electrical conductivity of the anatase electrode. The electrode synthesis parameters such as anodization potential, reduction potential, and time of reduction were optimized to get a kilohertz response pseudocapacitor. The kHz

pseudocapacitor displayed ability to retain capacitive behavior at high frequencies (190 $\mu\text{F cm}^{-2}$ at self resonance frequency (SRF) of 60 kHz) that is far superior to the kHz EDLCs (20 $\mu\text{F cm}^{-2}$ at 80 kHz SRF or 67 $\mu\text{F cm}^{-2}$ at 20 kHz SRF). The pseudocapacitor could filter a 50 kHz sinusoidal signal to a smooth line with a variance of less than 4×10^{-4} .

Keywords: Supercapacitors, electrochemical treatment, defect engineering, electrochemical energy storage, vertically oriented graphene nanoflakes, carbon fiber paper, anatase, kilohertz capacitor.

सार

सुपरकैपेसिटर विद्युत ऊर्जा भंडारण उपकरण का एक वर्ग है जो ए दिखाता है की संचित चार्ज की मात्रा के साथ क्षमता में भिन्नता होती है. यह आदर्श रूप से अनुकूल है अनुप्रयोगों में जहा पल्स पावर की आवश्यकता होती है, जैसे कि जेट विमानों में दरवाजे के आपातकालीन उद्घाटन, ऑटोमोबाइल में पुनर्योजी ब्रेकिंग, आदि. सुपरकैपेसिटर, कन्वेंशनल कैपेसिटर और बैटरीज के गैप को मिटाता है. डिएलेक्ट्रिक कपैसिटर के तुलना इसमें ज्यादा ऊर्जा घनत्व होता है और बैटरीज के तुलना ज्यादा पावर घनत्व और साइकिल क्षमता होती है. हालांकि छोटे ऊर्जा घनत्व के वजह से इसके प्रैक्टिकल एप्लिकेशन्स कम है. भविष्य के मॉडल पोर्टेबल और फ्लेक्सिबल उपकरणों के विकास के वजह से ऊर्जा स्टोरेज उपकरणों की डिमांड कन्टिन्यूसली बढ़ती जा रही है. सुपरकैपेसिटर ऊर्जा स्टोरेज में सुधार के लिए शोध मुख्य रूप से बेहतर इलेक्ट्रोड सामग्री विकसित करने पर केंद्रित है. रणनीतियों सुपरकैपेसिटर के प्रकार पर निर्भर करती हैं. इलेक्ट्रिक डबल लेयर कपैसिटर में शोध मैटेरियल्स का सरफेस एरिया और इलेक्ट्रिकल कंडक्टिविटी बढ़ाने पर केंद्रित है. वही सुडोकपैसिटर में सरफेस एरिया बढ़ाने के साथ सेमीकंडक्टर मटेरियल की कंडक्टिविटी बढ़ाना एक मुख्य उद्देश है. सुपरकैपेसिटर रिसर्च में उसका फ्रीक्वेंसी रिस्पांस बढ़ाना भी एक अहम् कार्य है. अधिकांश सुपरकैपेसिटर 5 हर्ट्ज तक ही फ्रीक्वेंसी तक ही कपैसिटिव बेहिवियर दिखाते है. एसी फिल्टर एप्लीकेशन के लिए एक सुपरकैपेसिटर की फ्रीक्वेंसी प्रतिक्रिया में सुधार की बहुत बड़ी गुंजाइश है.

इस काम में, एलेक्ट्रोकेमिकल ट्रीटमेंट और डिफेक्ट इंजीनियरिंग से सुपरकैपेसिटर ऊर्जा घनत्व (कुल वजन के आधार पर) और फ्रीक्वेंसी रिस्पांस में सुधार करने का लक्ष्य रखा है. पहले प्रायोगिक अध्ययन में, एक व्यावसायिक रूप से उपलब्ध हाइली ओरिएंटेड पैरोलीटिक ग्रेफाइट शीट को विभिन्न सल्फेट आयन आधारित इलेक्ट्रोलाइट्स में आंशिक रूप से एक्सफोलीएट किया गया था ताकि वर्टीकल ओरिएंटेड ग्राफीन, ग्रेफाइट सरफेस पर प्राप्त किया जा सके. प्रोसेस पैरामीटर्स जैसे की एक्सफोलिएशन का समय, करंट घनता , इलेक्ट्रोलाइट पीएच आदि को ऑप्टिमाइज़ किया. कम पीएच इलेक्ट्रोलाइट में एक्सफोलिएशन का रेट कम पाया गया और चार्ज स्टोर करने की क्षमता ज्यादा पायी गयी. यह पाया गया की इलेक्ट्रोड का एक्सपांशन, एनर्जी डेंसिटी बढ़ाने में एक महत्वपूर्ण रोल अदा करता है.

दो आयामी कार्बन में एक्सपांशन केवल एक ही दिशा में सिमित है , जब की कार्बन फाइबर इलेक्ट्रोड में तीन दिशा में एक्सपांशन की क्षमता है. इसलिए, मैंने अपने दूसरे अध्ययन में, इलेक्ट्रोड के रूप में कार्बन फाइबर पेपर का उपयोग किया है. कार्बन फाइबर का एलेक्ट्रोकेमिकल ट्रीटमेंट विभिन्न कॉन्सेंट्रेशन (1-14 मोलर)के सल्फुरिक एसिड में किया गया. किए गए कैरेक्टराइजेशन से पता चलता है कि सक्रिय ग्राफीन किनारों की संख्या बढ़ जाती है. साथ ही सरफेस में खुदरापन, क्रिस्टल स्ट्रक्चर में डिफेक्ट और ऑक्सीजन वेकन्सी को बढ़ाता है. यह बदलाव, प्रिस्टिन कार्बन फाइबर के मुकाबले ट्रीट किये हुए कार्बन फाइबर का सरफेस एरिया और एनर्जी स्टोरेज क्षमता को परिमाणक्रम बढ़ाता है. ऑप्टिमम कंडीशन में बढ़ा हुआ कैपासिटंस २.४७ फैरड पर सेंटीमीटर, २ मिलीएम्पियर पर सेंटीमीटर स्केअर करंट घनता पर पाया गया , जो की रिपोर्टेड संख्या से ५० गुना ज्यादा है.

तीसरा अध्ययन एनाटेस के कैपेसिटिव प्रदर्शन में सुधार पर था, यह एक कम लागत, विद्युत रासायनिक स्थिरता और उच्च सैद्धांतिक कैपासिटंस वाला सुडोकपैसिटिव मटेरियल है. इलेक्ट्रिकल कंडक्टिविटी में सुधार और नैनोस्ट्रक्चरिंग एक साथ किया गया. एक दो कदम हाइड्रोथर्मल मार्ग को फ्लोरीन तत्व के साथ एनटेज को डोप करने के लिए नियोजित किया गया था. इलेक्ट्रोकेमिकल कैरेक्टराइजेशन यह बताते हैं की निर्माण किये गए डिफेक्ट्स इलेक्ट्रॉनिक चार्ज करियर घनता और इलेक्ट्रिकल कंडक्टिविटी को परिमाणक्रम बढ़ाते हैं. यह ट्रीटमेंट सरफेस एरिया को भी अधिक बढ़ाता है. यह दो सुधार के वजह से प्रिस्टिन मटेरियल के मुकाबले कैपासिटंस को ३ से ४ गुना बढ़ता है.

मेरे अंतिम अध्ययन में, मेरा उद्देश्य एक किलोहर्ट्ज फ्रीक्वेंसी रिस्पांस सुडोकपैसिटिव निर्माण करना था. एक पतली, ओपन पोर् स्ट्रक्चर की एनटेज लेयर गो करने के लिए मैंने टाइटेनियम शीट को NH_4F इलेक्ट्रोलाइट में ऑक्सीडाइज किया. इलेक्ट्रिकल कंडक्टिविटी बढ़ाने के हेतु इलेक्ट्रोड को रिदुस किया. इलेक्ट्रोड सिंथेसिस के पैरामीटर्स जैसे की ऑक्सीडेशन वोल्टेज, ऑक्सीडेशन समय, रिडक्शन पोटेंशियल और टाइम को अनुकूलन किया. हमारे ऑप्टिमम सुडोकपैसिटिव की किलोहर्ट्ज फ्रीक्वेंसी पर कैपेसिटिव व्यवहार को बनाए रखने की क्षमता बहुत बढ़ गयी.

Contents

Abstract	ix
1 Introduction	1
1.1 Background	1
1.2 Capacitors and electrochemical capacitors	4
1.2.1 Electric double layer capacitor	6
1.2.2 Pseudocapacitor	9
1.3 Challenges in supercapacitor research	12
1.4 Research objectives	14
1.5 Thesis organization	15
2 Literature review	17
2.1 Historical overview	17
2.2 Performance of a supercapacitor	18
2.2.1 Electrolytes	19
2.2.1.1 Aqueous electrolytes	20
2.2.1.2 Organic electrolytes	20
2.2.1.3 Ionic liquids	21
2.2.1.4 Gel electrolytes	21
2.2.2 Materials for supercapacitor electrodes	22
2.2.2.1 Carbon based EDLC materials	22
2.2.2.2 Pseudocapacitive materials	25
2.3 Kilohertz frequency response supercapacitors	27
2.4 Summary	29

3	Partial exfoliation of HOPG	33
3.1	Introduction	34
3.2	Experimental methods	38
3.2.1	Electrochemical treatment of HOPG	38
3.2.2	Material characterizations	39
3.2.3	Electrochemical measurements	39
3.3	Results and discussions	40
3.3.1	Pre-intercalation versus direct exfoliation	41
3.3.2	Effect of different sulfate salts, and pH	47
3.3.3	Effect of exfoliation time	50
3.3.4	Electrochemical characterization of the electrode	54
3.3.5	EDLC performance	58
3.4	Conclusions	62
4	Electrochemical anodization of CFP	63
4.1	Introduction	64
4.2	Experimental methods	66
4.2.1	Materials and anodization of CFP	66
4.2.2	Material characterizations	66
4.2.3	Electrochemical measurements	67
4.3	Results and discussions	70
4.3.1	Structural characterizations	70
4.3.2	Electrochemical performance	76
4.4	Conclusions	84
5	Fluorine-doped anatase for pseudocapacitor electrode	85
5.1	Introduction	86
5.2	Experimental methods	88
5.2.1	Synthesis of sodium titanium oxide nanotubes and fluorine doping	88
5.2.2	Material characterizations	89
5.2.3	Electrochemical measurements	91
5.3	Results and discussions	93
5.3.1	Phase identification from XRD and Raman analyses	93
5.3.2	Morphology changes on HF treatment of pristine anatase	94
5.3.3	Fluorine doping on HF treatment	98

CONTENTS

5.3.4	Fluorine doping induced defects, shallow states, and electronic conductivity	104
5.3.5	Electrochemical characterization	106
5.4	Conclusions	119
6	A Kiloherz Frequency Response Pseudocapacitor	121
6.1	Introduction	122
6.2	Materials and methods	124
6.2.1	Synthesis and electrochemical reduction of porous titania layer	124
6.2.2	Material characterizations	125
6.2.3	Electrochemical measurements	126
6.3	Results and discussion	127
6.3.1	Structural and morphological characterization	127
6.3.2	Electrochemical characterization	133
6.4	Conclusions	146
7	Conclusions	147
A	Appendix A	151
B	Appendix B	157
C	Appendix C	161
D	Appendix D	167
	References	171

List of Figures

1.1	The Ragone plot for different electrochemical energy storage and conversion devices.	3
1.2	A schematic diagram of a dielectric capacitor.	5
1.3	A schematic diagram of a supercapacitor.	6
1.4	A schematic diagram of the physical picture envisaged in the different models for the electric double layer: (a) Helmholtz model, (b) diffuse layer model, and (c) Stern model. Part (c) also shows the IHP, and OHP envisaged in the current models for the electric double layer.	8
1.5	A schematic diagram of the different mechanisms of charge storage that show pseudocapacitive behavior: (a) underpotential deposition, (b) redox mechanism, and (c) intercalation confined to near surface region of the electrode.	11
3.1	SEM image of (a) the top view, and (b) the cross-view of the pristine HOPG electrode.	43
3.2	SEM image of (a) the top view, and (b) the cross-view of the electrode exfoliated using route-1 (ExGrNH-1 electrode).	43
3.3	SEM image of (a) the top view, and (b) the cross-view of the electrode exfoliated using route-2 (ExGrNH-2 electrode).	44
3.4	TEM images of two exfoliated, loose graphene nanoflakes.	44
3.5	The areal capacitance of pristine HOPG, ExGrNH-1, and ExGrNH-2 electrodes measured in 0.1 M ammonium sulfate solution. The areal capacitance of HOPG electrode is shown in the inset, as the values are much smaller than the other two electrodes. The uncertainty in the capacitance data was between 5.1% and 11.2%.	46

LIST OF FIGURES

3.6	The areal capacitance at different discharge current densities for the HOPG electrode obtained by (a) partial exfoliation in aqueous solutions of different sulfate salts (uncertainty in the capacitance data was between 4.3% and 17.5%), and (b) exfoliation in 1 M $(\text{NH}_4)_2\text{SO}_4$ solutions of different pH, and in 1 M H_2SO_4 (uncertainty in the capacitance values was between 7.5% and 13.9%)	48
3.7	The areal capacitance of the HOPG electrodes obtained by exfoliation for 1200 s in sulfuric acid solutions of different concentrations. The uncertainty in the capacitance data was between 2.6% and 14.9%.	50
3.8	Raman spectra of (a) HOPG, and electrodes exfoliated for different times in 1 M sulfuric acid solution, and (b) magnified view of the Raman G peak.	52
3.9	The XPS (a) survey spectrum for the partially exfoliated HOPG electrode, and (b) the high-resolution C1s peak.	53
3.10	Cyclic voltammograms acquired in 1 M sulfuric acid solution for (a) the pristine HOPG, EXFG300, EXFG600, EXFG900, and EXFG1200 electrodes at 20 mV s^{-1} scan rate, and (b) EXFG1200 electrode at different scan rates.	56
3.11	Electrochemical analysis in 1 M sulfuric acid solution: (a) GCD curves for EXFG1200 electrode at different discharge current densities, and (b) the areal capacitance values for the EXFG300, EXFG600, EXFG900, and EXFG1200 electrodes at different discharge current densities. The uncertainty in the capacitance values was between 1.6% and 8.1%.	57
3.12	The areal capacitance of EXFG1200 electrode for 5000 charge-discharge cycles.	59
3.13	Electrochemical analysis of the symmetric EDLC cell: (a) cyclic voltammograms at different scan rates, and (b) GCD plots at different discharge current densities.	60
3.14	A comparison of the volumetric capacitance of the EDLC fabricated in the present work with the literature data. The uncertainty in the capacitance values was between 5.1% to 10.7%.	61
3.15	Photographs showing (a) a circuit with two prototype EDLC cells in series connected to a LED, and (b) the EDLC cells lighting a LED. The video demonstration web link is: www.sciencedirect.com/science/article/pii/S0013468619318043	61

LIST OF FIGURES

4.1	(a) XRD patterns for pristine and anodized carbon fiber papers, and (b) the magnified view of the G-002 peak.	69
4.2	Raman spectra for the pristine and anodized carbon fiber papers: (a) full spectra, and (b) the magnified view of the G peak.	71
4.3	FESEM images of (a) pristine CFP, (b) magnified view of the carbon fiber shown in part (a), (c) CFP12M, and (d) magnified view of the carbon fiber shown in part (c).	72
4.4	(a) BET isotherms for pristine CFP, and CFP12M; and (b) ECSA of the pristine and anodized CFPs. Pristine CFP, 5M, 7M, 10M, 12M and 14 M electrodes show ECSA in the range of 3.32 – 4.67, 15.12 – 18.09, 23.92 – 27.71, 33.72 – 35.16, 77.89 – 81.57, and 66.12 – 71.96 cm ² , respectively.	74
4.5	High resolution XPS C1s peaks for (a) CFP1M, (b) CFP5M, (c) CFP10M, (d) CFP12M, and (e) CFP14M. The deconvoluted, five component peaks are also shown for each C1s peak.	75
4.6	Areal capacitance of electrodes synthesized by anodization of CFP in 5 M sulfuric acid solution at different anodization current densities. The areal capacitance value shown are for 2 mA cm ⁻² discharge current density. The uncertainty in the capacitance values was between 2.9% and 9.2%.	77
4.7	Electrochemical characterizations of the anodized CFP electrodes: (a) GCD curves for CFP12M electrode at different discharge current densities, and (b) areal capacitance of the electrodes synthesized by anodization of CFP in sulfuric acid solutions of different concentrations. The uncertainty in the capacitance values was between 2.2% and 9.5%.	78
4.8	Cyclic voltammogram for CFP12M electrode at 10 mV s ⁻¹ scan rate. 80	
4.9	The areal capacitance of CFP12M electrode for 5000 charge-discharge cycles.	81
4.10	The performance of the symmetric supercapacitor cell fabricated from CFP12M electrodes: (a) cyclic voltammograms at different scan rates, and (b) GCD curves at different discharge current densities.	82
4.11	A Ragone plot comparing the performance of the symmetric EDLC fabricated in the present work with the literature data.	83
5.1	A schematic of the electronic energy states for fluorine-doped anatase. 88	

5.2	A schematic diagram for the two-step modification process of pristine anatase. The first hydrothermal treatment in 10 M NaOH solution converts anatase to nanotubes of a different phase. The second-step of hydrothermal treatment in 2 M HF solution converts the nanotubes to anatase nanoparticles and introduces fluorine-doping.	89
5.3	XRD patterns for pristine and doped anatase as well as NT.	94
5.4	Structural characterization of pristine and doped anatase as well as NT: (a) full Raman spectra, and (b) a magnified view of the Raman E_{1g} peak showing blue shift on HF treatment.	95
5.5	HRTEM images of pristine anatase: (a) low resolution image of the particles with the SAED pattern in the inset, and (b) a high resolution image showing lattice fringes.	96
5.6	HRTEM images of NT: (a) low resolution image of NT with the SAED pattern shown in the inset, and (b) high resolution image NT showing lattice fringes.	96
5.7	HRTEM images of FNP24: (a) low resolution image with an inset containing the SAED pattern, and (b) a high resolution image showing lattice fringes.	97
5.8	N_2 adsorption isotherms at 77 K for pristine anatase and FNPs. . .	99
5.9	XPS survey spectrum for FNP24 showing the characteristic peaks of the different elements present in the material.	100
5.10	High resolution XPS F1s peak for (a) FNP15, (b) FNP18, (c) FNP20, and (d) FNP24.	101
5.11	X-band EPR spectra of the pristine and fluorine-doped anatase powders at 288 K.	103
5.12	The Mott-Schottky plots for pristine and fluorine-doped anatase at 5 kHz. The slope of the plots show n-type semi-conductor behavior and the change in the slope shows increase in the charge carrier density for the doped anatase.	104
5.13	The conductive AFM color plots for the local conductivity for (a) pristine anatase, (b) FNP15, (c) FNP20, and (d) FNP24.	105
5.14	The electrochemical characterization of the supercapacitive behavior of pristine and fluorine-doped anatase: (a) cyclic voltammograms for the materials at 10 mV s^{-1} , and (b) cyclic voltammograms at different scan rates for FNP24 electrode.	107

LIST OF FIGURES

5.15	A quantitative analysis of the diffusion-limited charge storage component of the FNPs: (a) variation of q_T with inverse square root of the sweep rate, and (b) contribution of C_o and C_i to the total specific capacitance. The uncertainty in the q_T values was between 4.2% and 11.9%.	109
5.16	Impedance analysis for the capacitance of the pristine anatase and FNPs: (a) the impedance data in form of the Nyquist plot, along with the inset showing the the equivalent circuit model used to interpret the data, and (b) the electric double layer and pseudocapacitive contributions to the total capacitance of the electrodes determined from the the equivalent circuit model.	111
5.17	A comparison of the performance of pristine and fluorine-doped anatase as supercapacitor electrode: (a) GCD curves at 6.5 A g^{-1} , and (b) a plot of the inverse of iR drop against electronic charge carrier density of the electrodes calculated from Mott-Schottky analysis. The uncertainty in the measured iR drop values was between 2.9% and 6.9%.	113
5.18	A comparison of the performance of pristine and fluorine-doped anatase as supercapacitor electrode: (a) the specific capacitance at different discharge current densities, and (b) the cyclic charge-discharge performance of the FNP24 electrode. The uncertainty in the capacitance values was between 3.7% and 7.9%.	115
5.19	Cyclic voltammograms at different scan rates for the symmetric pseudocapacitor fabricated from FNP24 electrodes.	116
5.20	The performance of the symmetric pseudocapacitor fabricated from FNP24 electrodes: (a) GCD curves, and and (b) specific capacitance at different discharge current densities. The uncertainty in the capacitance values was between 9.8% and 17.2%.	117
5.21	A Ragone plot comparing the power density and energy density of the symmetric pseudocapacitor fabricated from FNP24 electrodes, with the literature reported values for symmetric supercapacitor. . .	118
6.1	A schematic of anodization of titanium sheet to obtain a porous titania top layer.	125

LIST OF FIGURES

6.2	XRD patterns of the titanium sheet (pattern i), titania layer obtained by anodization at 50 V (pattern ii), after annealing the titania layer at 450° for 2 h (pattern iii), and after electrochemical reduction at -1.5 V for 3 min (pattern iv). The peak are marked * are for the anatase phase.	129
6.3	FESEM images of the top view of the titania layer synthesized by anodization of titanium sheet at (a) 20 V, (b) 50 V, (c) 30 V, (d) layer anodized at 50 V followed by annealing at 450°C for 2 h, and (e) the layer anodized at 50 V, annealed at 450°C for 2 h and then electrochemically reduced at -1.5 V for 3 min. Some of the remnants of the lumen of the nanotubes among the nanoparticles are marked in the FESEM images.	130
6.4	High resolution XPS Ti 2p peak for (a) EA-50 electrode, and (b) EAR-50 electrode.	132
6.5	Mott-Schottky plots for EA50 and EAR-50 electrodes.	133
6.6	A comparison of the electrochemical performance of the symmetric pseudocapacitors fabricated from EA-50 and EAR-50 electrodes: (a) variation of phase angle with frequency, (b) Nyquist plot, (c) the equivalent circuit used to fit the experimental data, (d) variation of areal capacitance of the pseudocapacitors with frequency, and (e) variation of complex capacitance components (real: C' ; imaginary: C'') with frequency. The inset in the Nyquist plot shows the nearly vertical line nature of the plots near x-axis intersection. The equivalent circuit model simulated values are given as solid curves in part a, b and e.	134
6.7	A comparison of the electrochemical performance of the symmetric pseudocapacitors fabricated from the electrodes anodized at different potentials between 20 V and 60 V: (a) variation of areal capacitance with frequency, and (b) variation of phase angle with frequency.	137
6.8	Chronoamperograms for the cathodic reduction of EA-50 electrodes at different potentials.	138
6.9	A comparison of the electrochemical performance of the symmetric pseudocapacitors fabricated from electrodes anodized at 50 V for 50 min and reduced at different potentials between -1.0 V and -2.0 V for 10 min: (a) variation of areal capacitance with frequency, and (b) variation of phase angle with frequency.	139

LIST OF FIGURES

6.10	A comparison of the electrochemical performance of the symmetric pseudocapacitors fabricated from electrodes anodized at 50 V for 50 min and reduced at -1.5 V for different times: (a) variation of areal capacitance with frequency, and (b) variation of phase angle with frequency.	140
6.11	Variation of impedance with frequency for the EAR-50 electrode symmetric pseudocapacitor. The self resonance frequency (minimum impedance value) is shown in the plot.	143
6.12	Filtering performance of the EAR-50 electrode symmetric pseudocapacitor: (a) a schematic representation of the circuit used for full wave rectification of the sinusoidal input signal followed by filtering by the pseudocapacitor with a resistive load of $10\text{ k}\Omega$, (b) the filtered output (orange line) for a 60 Hz sinusoidal signal (green curve), and (c) the filtered output (orange line) for a 50 kHz sinusoidal signal (green curve).	144
A.1	GCD curves at 2 mA cm^{-2} discharge current density for ExGrNH-1, and ExGrNH-2 electrodes in 1 M ammonium sulphate solution.	152
A.2	GCD curves at 2 mA cm^{-2} discharge current density for electrode synthesized by partial exfoliation in aqueous solutions of different sulfate salts.	152
A.3	GCD curves at 2 mA cm^{-2} discharge current density for the electrodes synthesized by partial exfoliation of HOPG in 1 M sulfuric acid, 1 M ammonium sulfate solutions of pH 1 and 1 M ammonium sulfate solutions of pH 10.	153
A.4	A snapshot of the electrochemical exfoliation process in 1 M sulfuric acid solution at (a) 0 s , (b) 300 s , (c) 600 s , (d) 900 s , and (e) 1200 s	154
A.5	Raman spectra of electrode obtained by partial exfoliation of HOPG in ammonium sulfate solution for 300 s and 1200 s	154
A.6	Magnified view of the Raman G peak: (a) HOPG, (b) EXFG300, (c) EXFG600, and (d) EXFG1200 electrodes. The deconvoluted doublet peaks for the exfoliated electrodes are also shown.	155
B.1	The Raman G peak along with its deconvolution into the G main peak and the D' peaks for (a) CFP1M, (b) CFP5M, (c) CFP7M, and (d) CFP12M electrodes.	158

LIST OF FIGURES

B.2	GCD curves at 7 mA cm^{-2} discharge current density for the CFP treated electrochemically in different concentrations of H_2SO_4 . . .	159
B.3	Cyclic voltammograms at 10 mV s^{-1} scan rate for the electrodes obtained by anodization of CFP in sulfuric acid solutions of different concentrations.	159
B.4	Cyclic voltammograms at different scan rates for CFP12M electrode.	160
C.1	Indexed XRD pattern of NT.	162
C.2	Low resolution TEM image showing FNP24 particles of different shapes.	162
C.3	HRTEM images of the FNP15 powder: (a) low resolution image of the particles with the SAED pattern in the inset, and (b) high resolution image of showing lattice fringes.	163
C.4	HRTEM images of the FNP18 powder: (a) low resolution image of the particles with the SAED pattern in the inset, and (b) high resolution image of showing lattice fringes.	163
C.5	HRTEM images of the FNP20 powder: (a) low resolution image of the particles with the SAED pattern in the inset, and (b) high resolution image of showing lattice fringes.	164
C.6	Electrochemical characteristics of the graphite substrate used for pristine anatase and FNP electrodes: (a) cyclic voltammograms at different scan rates, and (b) GCD curves at different current densities. The curves were acquired in M sulfuric acid solution in a three-electrode set-up.	164
D.1	FESEM image of the electrode (a) anodized at 50 V and then reduced at -1.5 V without annealing, and (b) anodized at 50 V, annealed and then reduced at -2.0 V for 10 min.	167
D.2	FESEM cross-view images of the titania layer obtained at anodization potential of (a) 60 V, (b) 60 V magnified view, (c) 50 V, and (d) 50 V magnified view.	168
D.3	EDX spectrum for (a) EA-50, and (b) EAR-50 electrode.	168
D.4	XPS survey spectra for EAR-50 electrode	169

LIST OF FIGURES

D.5 Impedance versus frequency plots for the EAR-50 electrode pseudo-capacitor with different upper limit of the frequency: (a) 100 kHz, (b) 300 kHz, (c) 500 kHz, and (d) 700 kHz. The increase in the magnitude of impedance, a mark of the dominance of the inductive character of the device is clearly visible for upper frequency limit of 300 kHz or higher values.	170
--	-----

List of Tables

1.1	A comparison of the properties of a battery, a capacitor and a supercapacitor	4
2.1	A comparison of the figures of merit of the high frequency response EDLCs fabricated using different electrode materials.	31
3.1	A comparison of the ECSA for the partially exfoliated HOPG electrodes.	45
3.2	A comparison of the areal capacitance of the electrodes with VOG nanoflakes morphology grown at different conditions.	55
4.1	A comparison of the capacitance of the carbon fiber paper or VOG nanoflakes based supercapacitor electrodes.	79
5.1	Surface area and pore volume of the pristine and fluorine-doped anatase powders measured using the BET method.	99
5.2	The relative proportion of fluorine in three different chemical states, calculated from area of the component peaks.	102
6.1	The phase angle and areal capacitance at 120 Hz for the symmetric pseudocapacitors fabricated from electrodes reduced at -1.5 V for different times.	136
6.2	A comparison of the figures of merit for the kHz EDLCs comprising of different carbon-based electrodes with the kHz anatase pseudocapacitor	145
A.1	Properties of highly oriented pyrolytic graphite (HOPG) sheet, purchased from Nickunj Eximp India Pvt. Ltd., India.	151

LIST OF TABLES

B.1	Properties of carbon fiber paper purchased from Global Nanotech, India.	157
B.2	A comparison of the ratio of the intensity of D' peak to G peak of the Raman spectra for the anodized carbon fiber paper.	158
B.3	The relative composition of the different oxygen functional groups for the anodized carbon fiber paper. The values are calculated from the area of the deconvoluted component peaks of C1s XPS peak. . .	160
C.1	The retention of the capacitance (in percent) for the pristine anatase and different FNP electrodes on increasing the discharge current density from 1.5 A g^{-1} to 8 A g^{-1}	161
C.2	The best-fit parameters of the equivalent circuit model used to describe the impedance spectra of anatase and FNP electrodes. . . .	165
D.1	The best-fit parameters of the equivalent circuit model used to model the impedance spectra of EA-50 and EAR-50.	169

Nomenclature and list of abbreviations

Symbol	Definition
A	Area of electrode (cm^{-2})
C	Capacitance (F)
C_{dl}	Specific double layer capacitance (F g^{-1})
C_{ps}	Specific pseudocapacitance (F g^{-1})
C_A	Areal capacitance (mF cm^{-2} or F cm^{-2})
C_{Fe}	Concentration of the ferricyanide ion (mM)
C_i	Specific capacitance due to less-accessible inner surface (F g^{-1})
C_o	Specific capacitance due to easily accessible outer surface (F g^{-1})
C_{sp}	Specific capacitance (F g^{-1})
C_V	Volumetric capacitance (F cm^{-3})
C'	Real component of complex capacitance (F)
C''	Imaginary component of complex capacitance (F)
D	Diffusion coefficient of ferricyanide ($\text{m}^2 \text{s}^{-1}$)
E	Applied bias potential, Electrode potential (V)
E_i	Initial potential of the discharge curve (V)
E_f	Final potential of the discharge curve (V)
e	Electron charge (C)
ESR	Equivalent series resistance (Ω)
ΔE	Voltage window (V)
$\frac{\Delta E}{\Delta t}$	Slope of discharge curve (mV s^{-1})
f_0	Frequency at maximum C'' (Hz)

LIST OF TABLES

I	Constant discharge current (mA)
i_p	Peak current (mA)
iR_{drop}	Difference between final charge voltage and first point in discharge curve
m	Mass of an electrode (mg)
N_d	Charge carrier density (cm^{-3})
P	Power density of the device (W kg^{-1})
q_T	Total charge stored (C)
q_i	Charge stored by the less accessible surface (C)
q_o	Charge stored by the easily accessible outer surface (C)
R_{ESR}	Equivalent series resistance (Ω)
t	discharge time (s)
U	Energy density of the device (Wh kg^{-1})
V	Volume of the device (cm^{-3})
v	Scan rate (mV s^{-1})
Z'	Real part of impedance (Ω)
Z''	Imaginary part of impedance (Ω)
ϵ_0	Permittivity of vacuum (F m^{-1})
ϵ_r	Relative permittivity
τ_{RC}	Resistance time constant (ms)

Abbreviation Description

AcC	Activated carbon
AEC	Aluminum electrolytic capacitor
ASC	Asymmetric supercapacitor
BDM	Bockris, Devanathan, and Muller
BET	Brunauer-Emmett-Teller
C-AFM	Conductive atomic force microscopy
CDC	Carbide derived carbon
CFP	Carbon fiber paper
CNT	carbon nanotube
CV	Cyclic voltammetry or cyclic voltammogram
CVD	Chemical vapor deposition
EA	Electrochemically anodized electrode
EAR	Electrochemically anodized and then reduced electrode

LIST OF TABLES

ECSA	Electrochemical surface area
EDL	Electric double layer
EDX	Energy-dispersive X-ray spectroscopy
EDLC	Electric double layer capacitor
EED	Energy conversion and storage devices
EES	Electrochemical energy conversion and storage devices
EIS	Electrochemical impedance spectroscopy
EPR	Electron paramagnetic resonance spectroscopy
ESR	Equivalent series resistance
EV	Electric vehicle
ExGrNH-1	Electrode exfoliated in $(\text{NH}_4)_2\text{SO}_4$ by route 1
ExGrNH-2	Electrode exfoliated in $(\text{NH}_4)_2\text{SO}_4$ by route 2
FESEM	Field emission scanning electron microscopy
EXFG	Exfoliated graphite sheet
FLG	Few layer graphene
FNP	Fluorine doped nanoparticles
GCD	Galvanostatic charge-discharge
GO	Graphene oxide
HOPG	Highly oriented pyrolytic graphite
HRTEM	High resolution transmission electron microscopy
IHP	Inner Helmholtz plane
iOT	Internet of things
MO	Metal oxides
OHP	Outer Helmholtz plane
PECVD	Plasma enhanced chemical vapor deposition
PEDOT	Poly(3,4-ethylenedioxythiophene)
RGO	Reduced graphene oxide
SAED	Selected area electron diffraction
SHE	Standard hydrogen electrode
SSC	Symmetric supercapacitor
TNT	Titania nanotube
VOG	Vertically oriented graphene
XPS	X-ray photoelectron spectroscopy
XRD	X-ray diffraction